

## Evaluation of the Vegetated Urban Canopy Model (VUCM) and Its Impacts on Urban Boundary Layer Simulation

Sang-Hyun Lee<sup>1</sup> and Jong-Jin Baik

School of Earth and Environmental Sciences, Seoul National University, Seoul, Korea

<sup>1</sup>Current affiliation: Chemical Sciences Division, NOAA Earth System Research Laboratory, Boulder, Colorado, U.S.A.

(Manuscript received 25 June 2010; revised 20 October 2010; accepted 19 November 2010)  
© The Korean Meteorological Society and Springer 2011

**Abstract:** The vegetated urban canopy model (VUCM) is implemented in a meteorological model, the Regional Atmospheric Modeling System (RAMS), for urban atmospheric modeling. The VUCM includes various urban physical processes such as in-canyon radiative transfer, turbulent energy exchanges, substrate heat conduction, and in-canyon momentum drag. The coupled model RAMS/VUCM is evaluated and then used to examine its impacts on the dynamic and thermodynamic structure of the urban boundary layer (UBL) in the Seoul metropolitan area. The spatial pattern of the nocturnal urban heat island (UHI) in Seoul is quite well simulated by the RAMS/VUCM. A statistical evaluation of 2-m air temperature reveals a significant improvement in model performance, especially in the nighttime. The RAMS/VUCM simulates the diurnal variations of surface energy balance fluxes realistically. This contributes to a reasonable UBL formation. A weakly unstable UBL is formed in the nighttime with UBL heights of about 100–200 m. When urban surfaces are represented in the RAMS using a land surface model of the Land Ecosystem-Atmosphere Feedback (LEAF), the RAMS/LEAF produces strong cold biases and thus fails to simulate UHI formation. This is due to the poor representation or absence of important urban physical processes in the RAMS/LEAF. This study implies that urban physical processes should be included in numerical models in order to reasonably simulate meteorology and air quality in urban areas and that the VUCM is one of the promising urban canopy models.

**Key words:** Vegetated urban canopy model, urban boundary layer, urban heat island, surface energy balance, urban atmospheric modeling

### 1. Introduction

Urbanized areas occupy less than 0.1% of the earth's surface, but over 50% of the global population lives in cities (United Nations, 2004). The anthropogenic forcing by human activities is accelerating global/urban warming and deteriorating air quality, consequently threatening human health and urban sustainability. To cope with issues associated with urbanization, it is necessary to understand the dynamics and thermodynamics of the urban boundary layer (UBL), which forms by mechanical and thermal influences of urban surfaces (Garratt, 1992). Urban surfaces are typically composed of artificial surfaces (e.g., buildings, roads) and vegetated surfaces (e.g., parks, trees). In

conjunction with complex urban morphology, large roughness length, low albedo, large thermal inertia, and low moisture availability, urban physical processes result in the characteristic features of mean flow, turbulence, and thermal structure in the UBL. These features were observed in many field measurements and wind-tunnel experiments (e.g., Dupont *et al.*, 1999; Feigenwinter *et al.*, 1999; Kastner-Klein *et al.*, 2001; Allwine *et al.*, 2002; Grimmond and Oke, 2002; Mestayer *et al.*, 2005).

Urban physical processes are very complex and their interactions are highly nonlinear. Meteorological models have been widely used for urban atmospheric modeling. Traditionally, urban surfaces in meteorological models have been represented in an approach similar to that used to represent natural surfaces which employs a ‘big leaf’ concept (e.g., Deardorff, 1978; Sellers *et al.*, 1996; Dickinson *et al.*, 1998; Walko *et al.*, 2000). In the traditional approach of urban surface representation, urban physical processes are not explicitly represented. Previous studies have tried to mimic the structure of the UBL by changing physical parameters such as roughness length, vegetation fraction, and leaf area index. However, due to poor representation or absence of some important urban physical processes, the traditional approach frequently fails to realistically simulate the urban surface energy balance and UBL structure (e.g., Best *et al.*, 2006).

As one of the recent efforts for realistic urban numerical modeling, urban canopy models have been developed (Masson, 2000; Kusaka *et al.*, 2001; Martilli *et al.*, 2002; Lee and Park, 2008; Oleson *et al.*, 2008). Lee and Park (2008) developed a vegetated urban canopy model (VUCM) for use in mesoscale meteorological and environmental modeling. In the VUCM, various physical processes such as in-canyon radiative transfer, turbulent energy exchanges, substrate heat conduction, and in-canyon momentum drag are explicitly included. Physical processes associated with artificial surfaces and vegetated surfaces are parameterized in an integrated system.

In this study, the VUCM is implemented in a meteorological model for high-resolution urban numerical modeling and the coupled model is evaluated using surface meteorological data. Then, the impacts of the VUCM on the UBL are investigated. The region of our interest is the Seoul metropolitan area. Section 2 describes the meteorological model, the land surface model, the VUCM, and an implementation of the VUCM in the meteorological model. Section 3 presents a case selected and

Corresponding Author: Jong-Jin Baik, School of Earth and Environmental Sciences, Seoul National University, Seoul 151-742, Korea.  
E-mail: jjbaik@snu.ac.kr

experimental setup. Section 4 presents and discusses evaluation and simulation results. Summary and conclusions are given in section 5.

## 2. Model description and coupling

### a. Meteorological model

The Regional Atmospheric Modeling System (RAMS) version 4.4 is used in this study, which is a three-dimensional, nonhydrostatic, compressible primitive equation model (Pielke *et al.*, 1992). The RAMS uses an Arakawa-C grid system with a terrain-following vertical coordinate and has a two-way nesting capability. The RAMS includes various physical parameterizations of subgrid-scale turbulent mixing, subgrid-scale and grid-scale convection, radiation, and land surface processes. The RAMS has been used for a wide range of meteorological simulations and applications (e.g., Lyons *et al.*, 1995; McQueen *et al.*, 1997; Jiang and Cotton, 2000; Walko *et al.*, 2000; Zhong and Fast, 2003).

### b. Land surface model

The RAMS includes a land surface model of the Land Ecosystem-Atmosphere Feedback (LEAF), which provides bottom boundary conditions for the RAMS (Lee and Pielke, 1992). The LEAF is a soil-vegetation-atmosphere energy and momentum transfer scheme, in which conservation equations for energy and momentum are applied to vegetation, canopy air, and soil layers in each patch of a grid cell (Walko *et al.*, 2000). Various physical processes such as turbulent exchange, heat conduction, water diffusion and percolation in soil layers, longwave and shortwave radiative transfer, transpiration, and precipitation are considered for mass and energy exchanges. The LEAF allows multiple surface types to coexist in a single grid cell in order to represent fine-scale variations in landuse types. Each patch is represented by a fractional area occupied by its particular landuse type in a grid cell. Each patch consists of its own soil layers, vegetation, and canopy air. All patches interact with the same overlying air (reference forcing level) for the turbulent exchanges of momentum, heat, and water (Walko *et al.*, 2000). This approach, called the mosaic approach, is of benefit in representing spatial heterogeneity in a grid cell (Avissar and Pielke, 1989). Details of the LEAF are described in Lee and Pielke (1992) and Walko *et al.* (2000).

Urban processes in the LEAF follow the same physical parameterizations used for natural surface types. An urban patch is represented by the parameters of soil and vegetation, which are altered ('tuned') to give reasonable turbulent fluxes in urban areas. The LEAF does not consider urban morphological features and their associated physical processes.

### c. Vegetated urban canopy model

The VUCM is a single-layer urban canopy model developed

for use in mesoscale meteorological and environmental modeling. The VUCM calculates turbulent exchanges of momentum, heat, and moisture for the bottom boundary conditions of meteorological models. Figure 1 shows the schematic diagram of the VUCM. In the VUCM, an urban patch is represented by a simple urban canopy composed of canyon and building. The canyon bottom surface is divided into an impervious surface (road) and a vegetated surface (tree and soil). Turbulent exchange processes are associated with in-canyon radiative transfer, heat conduction in the substrate of artificial surfaces, heat and hydraulic conduction in soil layers, and hydrological processes (precipitation, evaporation, dewfall, and transpiration). Five energy exchanging surfaces (roof, wall, road, soil, and vegetation) are influenced interactively. The VUCM is capable of simulating urban effects such as radiation trapping, shadowing, heat storage, and in-canyon wind speed reduction. A stand-alone version of the VUCM was evaluated using the Vancouver field measurements, focusing on nocturnal radiative cooling, and the Marseille field measurements, focusing on the overall model performance under fair weather conditions. A detailed description of the VUCM is given in Lee and Park (2008).

### d. Coupling the VUCM to the RAMS

The VUCM is forced by downward shortwave and longwave radiative fluxes, wind speed, temperature, specific humidity, and

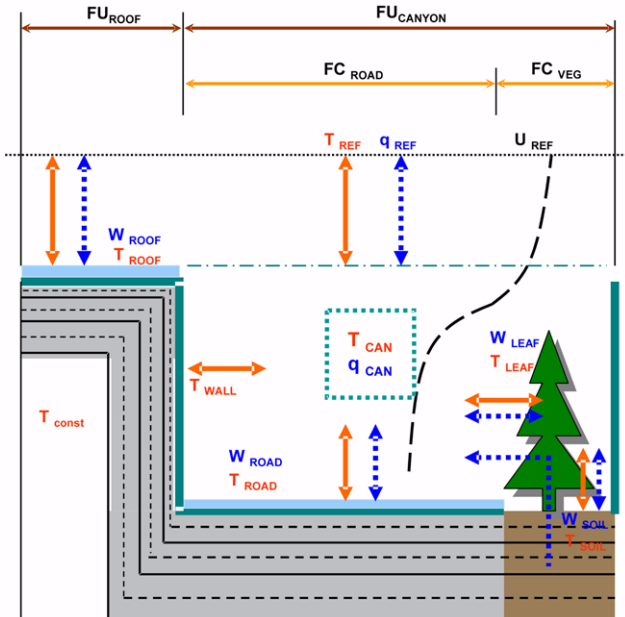


**Fig. 1.** Schematic diagram of the vegetated urban canopy model (VUCM). Solid and dotted arrows indicate sensible heat and moisture exchange pathways, respectively (from Lee and Park, 2008). T, q, U, and W indicate the temperature, specific humidity, wind speed, and water amount, respectively. The subscript REF represents a reference level, and the subscript CAN represents the canopy air. FU<sub>ROOF</sub> and FU<sub>CANYON</sub> indicate the fractions of roof and canyon in an urban patch, and FC<sub>ROAD</sub> and FC<sub>VEG</sub> indicate the fractions of road and vegetated area within the canyon.

precipitation at a reference level. Given the meteorological forcing, the VUCM calculates upward shortwave and longwave radiation, momentum flux, sensible heat flux, and moisture flux over an urban patch. A coupling between the VUCM and the RAMS is done in a manner that the RAMS provides required meteorological variables (forcing) to the VUCM and then the VUCM calculates and provides the boundary conditions of momentum, heat, and moisture fluxes. When a grid cell in the RAMS is occupied with both urban and natural surfaces with each area fraction of  $A_i$  ( $\sum_{i=1}^N A_i = 1$ ), the VUCM and the LEAF calculate radiative and turbulent fluxes separately for the urban and natural surfaces. Once the fluxes of each patch are calculated, the resultant fluxes in a grid cell are weight-averaged by the area

fractions of corresponding patches. The integrated vertical momentum fluxes, heat flux, and moisture flux are computed using

$$\overline{(u'w')}_0 = -\left(\frac{u}{\sqrt{u^2+v^2}}\right) \sum_{i=1}^N A_i (u_*^2)_i, \quad (1)$$

$$\overline{(v'w')}_0 = -\left(\frac{v}{\sqrt{u^2+v^2}}\right) \sum_{i=1}^N A_i (u_*^2)_i, \quad (2)$$

$$\overline{(w'\theta')}_0 = \sum_{i=1}^N A_i (u_* \theta_*)_i, \quad (3)$$

$$\overline{(w'r')}_0 = \sum_{i=1}^N A_i (u_* r_*)_i. \quad (4)$$

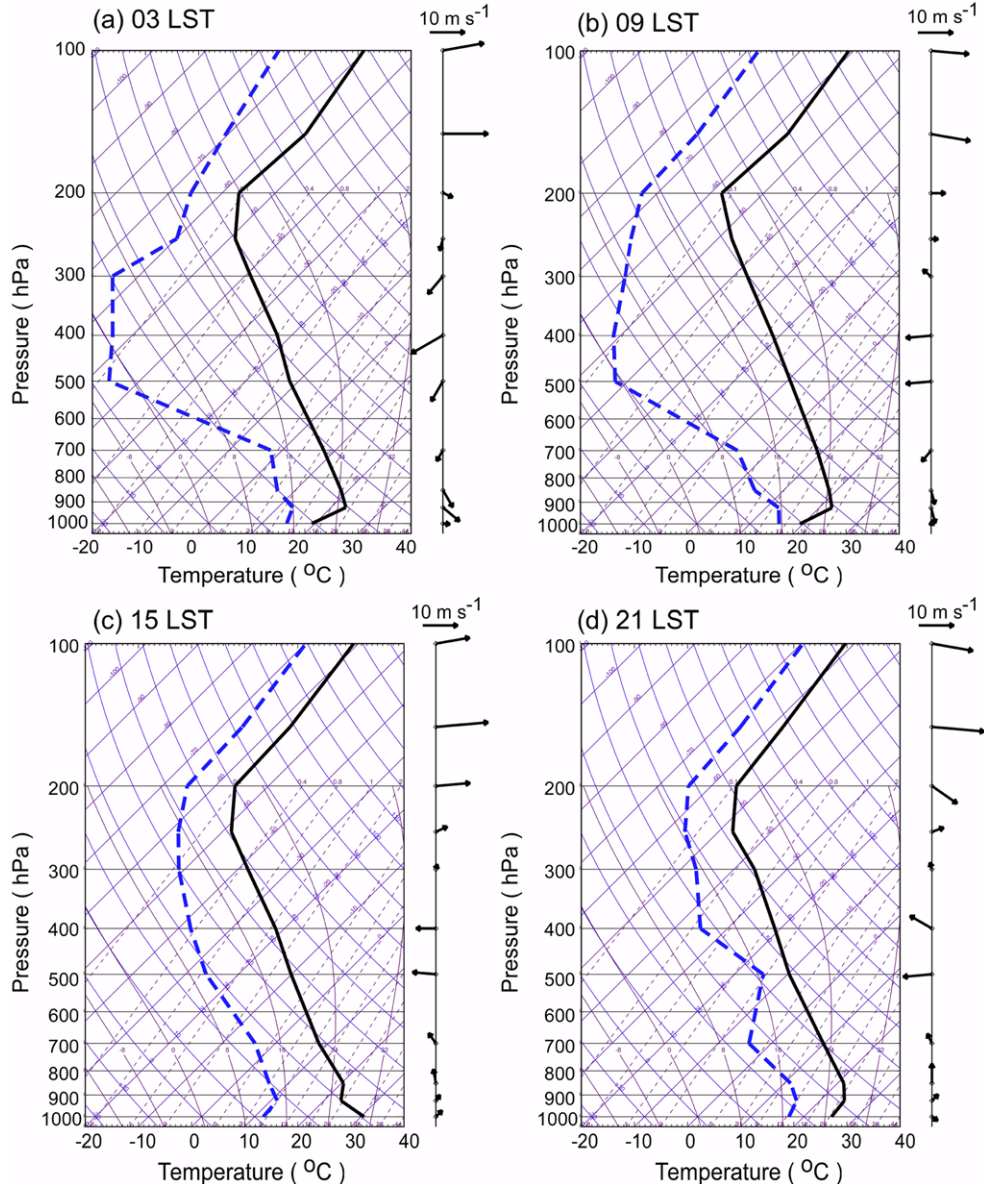


**Fig. 2.** Skew  $T$ -log  $p$  diagrams obtained from the Osan soundings at (a) 0300 LST, (b) 0900 LST, (c) 1500 LST, and (d) 2100 LST 7 June 2001. The solid and dashed lines indicate the temperature and dew point temperature, respectively.

Here,  $u_*$ ,  $\theta_*$ , and  $r_*$  are the friction velocity, the temperature scale, and the moisture scale computed from the surface-layer similarity theory,  $u$  and  $v$  are the horizontal velocity components,  $w$  is the vertical velocity component,  $\theta$  is the potential temperature,  $r$  is the water vapor mixing ratio, and  $N$  is the number of patches in a grid cell. It is noted that the integrated surface momentum flux is partitioned into  $u$ - and  $v$ -component in proportion to the wind speed in each direction at a reference level according to the surface-layer similarity theory [Eqs. (1) and (2)].

### 3. Case-day selection and experimental setup

In order to evaluate the VUCM and examine its impacts on boundary layer simulated for the Seoul metropolitan area, we select a clear summer day with a weak synoptic forcing (7 June 2001), thereby local circulations such as land/sea breezes and mountain/valley winds being predominant. Skew  $T$ -log  $p$  diagrams obtained from the Osan soundings at 03, 09, 15, and 2100 LST 7 June 2001 are shown in Fig. 2 in order to represent synoptic meteorological conditions of the selected day over the area of interest. The Osan radiosonde station ( $37.091^{\circ}\text{N}$ ,  $127.030^{\circ}\text{E}$ ) is one of the operational radiosonde stations in Korea and has the World Meteorological Organization (WMO) station code of 47122. At 850 hPa, the wind speed was less than  $5 \text{ m s}^{-1}$  during the day and the wind direction changed clockwise from northwesterly at 0300 LST to southerly at 2100 LST. During the day, the atmospheric stability in the lower layer from 900 hPa to 700 hPa was about  $6 \text{ K km}^{-1}$  and the vertical wind shear in the lower layer was very weak by about  $0.001 \text{ s}^{-1}$ . The surface mean wind speed in the finest domain (Fig. 3) was about  $1.4 \text{ m s}^{-1}$ . The cloud amount measured at meteorological stations in the Seoul metropolitan area was less than three tenths. The estimated maximum urban heat island (UHI) intensity was about  $3^{\circ}\text{C}$ , which is comparable to the mean maximum UHI intensity in summer ( $3.5^{\circ}\text{C}$ ) (Lee and Baik, 2010). Here, following Lee and Baik (2010), the UHI intensity is defined as a difference between the temperature averaged over the five urban stations

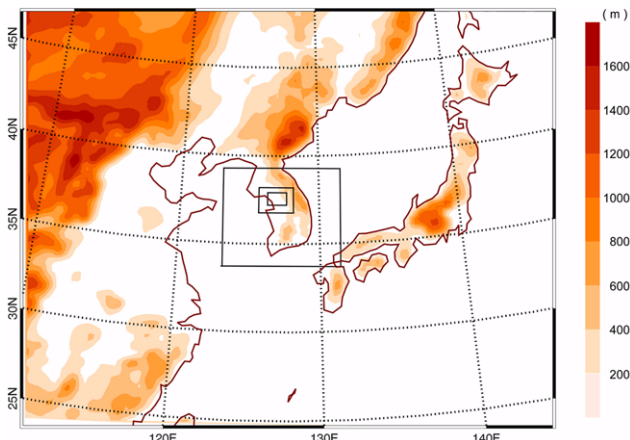


**Fig. 3.** Configuration of nested model domains. Topography is shaded with intervals of 200 m. The Seoul metropolitan area is located within the finest domain.

and the temperature averaged over the six rural stations. The observed maximum incoming solar radiation was about  $830 \text{ W m}^{-2}$ . The meteorological conditions of the day were favorable for intense surface turbulent energy exchanges, thus promoting thermally induced local circulations.

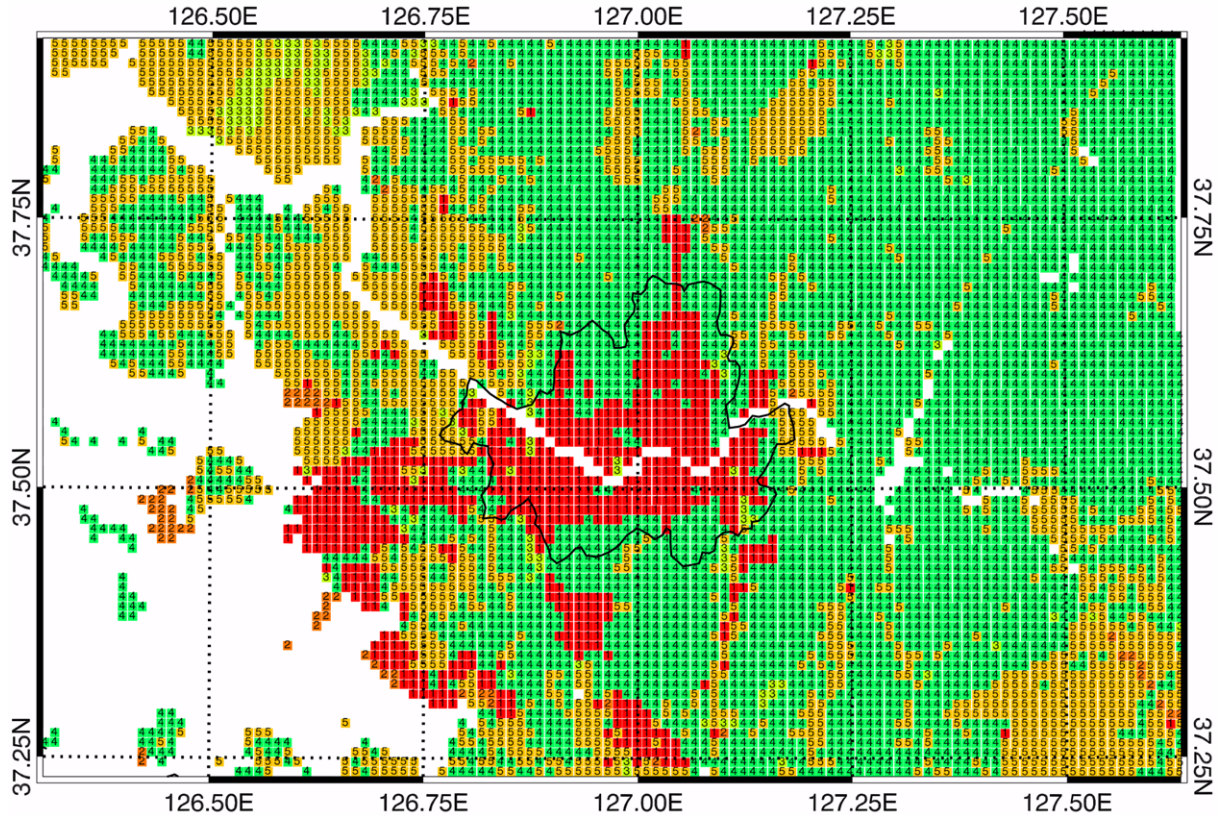
In this study, two simulations are conducted with the coupled model RAMS/VUCM and the original RAMS model RAMS/LEAF. The only difference between the two simulations lies in urban parameterization. For an urban patch, the VUCM and the LEAF are used in the RAMS/VUCM and RAMS/LEAF simulations, respectively. For a non-urban patch, the LEAF is used to calculate surface fluxes in both the simulations. The anthropogenic heat flux is not included in the simulations.

Four computational domains are configured, and the simulations are conducted using a two-way nesting approach (Fig. 3). The coarsest domain has  $120 \times 100$  mesh with a horizontal grid spacing of 27 km, covering the eastern China, the Korean peninsula, and Japan. The nesting ratio in horizontal grid spacing is set to be three for all domains. The finest domain has  $122 \times 80$  mesh with a horizontal spacing of 1 km, covering the Gyeong-In region where the Seoul metropolitan area is located. The vertical grid system is composed of 41 levels, stretching from near surface ( $\sim 16 \text{ m}$ ) to the model top ( $\sim 20 \text{ km}$ ) with a stretching ratio of 1.15. Subgrid-scale cumulus convection is parameterized using the modified Kuo scheme (Tremback, 1990), and it is applied only for the coarsest domain. Grid-scale clouds are parameterized using a one-moment bulk cloud microphysics scheme, in which eight water species (water vapor, cloud, rain, pristine ice, snow, aggregate, graupel, and hail) are considered. The Mellor-Yamada level 2.5 turbulence scheme (Heldman and Labraga, 1988) is used for vertical turbulent diffusion. The predicted turbulent kinetic energy (TKE) is used to calculate the atmospheric boundary layer height diagnostically. Shortwave and longwave radiation is calculated following Chen and Cotton (1983), in which cloud and topography slope effects are taken into account. The lateral boundary condition proposed by Davies (1976) is used. The outermost five grid points are nudged using large-scale analysis fields. The initial and boundary conditions for wind, temperature, and humidity are produced using the National Centers for Environmental Prediction (NCEP) final analysis (FNL) data ( $1^{\circ} \times 1^{\circ}$ ) with 6-hr intervals. These fields are nudged during the first three hours for all domains. Sea surface temperatures are obtained from the National Oceanic and Atmospheric Administration (NOAA)/National Aeronautics and Space Administration (NASA) Advanced Very High Resolution Radiometer (AVHRR) Oceans Pathfinder data with a spatial resolution of 4 km ([ftp://podaac.jpl.nasa.gov/documents/dataset\\_docs/avhrr\\_pathfinder\\_sst.html](ftp://podaac.jpl.nasa.gov/documents/dataset_docs/avhrr_pathfinder_sst.html)). It is assumed that sea surface temperatures remain constant during the simulation. The RAMS is integrated for 28 hours starting from 2100 LST 06 June 2001. A summary of experimental setup for the simulations is given in Table 1.

The RAMS represents the subgrid-scale heterogeneity of landuse types using the mosaic approach in filling up a grid cell (Avissar and Pielke, 1989; Walko *et al.*, 2000). As the horizontal

**Table 1.** Experimental setup for the simulations.

Category	Setup
Governing equations	3-dimensional, nonhydrostatic, compressible
Horizontal grid structure	Arakawa-C grid, two-way nesting
Vertical coordinate	Terrain-following sigma $z$
Horizontal spacing	Domain 1: $\Delta x = \Delta y = 27$ km ( $120 \times 100$ ) Domain 2: $\Delta x = \Delta y = 9$ km ( $80 \times 74$ ) Domain 3: $\Delta x = \Delta y = 3$ km ( $74 \times 53$ ) Domain 4: $\Delta x = \Delta y = 1$ km ( $122 \times 80$ )
Vertical spacing	Variable $\Delta z$ , 41 levels Lowest level: 16.3 m, model top height: ~20 km
Grid-scale clouds	One-moment bulk microphysics
Subgrid-scale clouds	Modified Kuo scheme (Tremback, 1990)
Turbulence	Mellor-Yamada level 2.5 scheme (Held and Labraga, 1988)
Radiation	Shortwave and longwave radiation (Chen and Cotton, 1983)
Land surface process	LEAF-2 (Walko <i>et al.</i> , 2000), VUCM for urban patches
Initial and boundary conditions	NCEP final analysis (FNL) data, Nudging using outermost 5 points (Davies, 1976)
Integration	28 hr

**Fig. 4.** Spatial distribution of dominant landuse types in the finest domain. The landuse types are denoted by numbers (colors) : 1 for urban area (red), 2 for bare ground (brown), 3 for grassland (light green), 4 for forest (green), and 5 for crop/mixed farming (yellow). Seoul administrative boundary is marked by solid line.

grid spacing decreases, surface heterogeneity can be resolved without sub-patches. In this study, two landuse types are allowed in a grid cell with their fractional coverage areas. Figure 4 shows

the spatial distribution of dominant landuse types in the finest domain. Urban areas are remapped using landuse data with a spatial resolution of 30 m (data from the Korea Ministry of

**Table 2.** LEAF parameters used for each landuse type. The listed landuse types are the same as in Fig. 4.

Parameters	Unit	Urban	Bare ground	Grassland	Forest	Crop/mixed farming
Albedo ( $\alpha$ )		0.15	0.16	0.11	0.07	0.20
Emissivity ( $\varepsilon$ )		0.90	0.86	0.96	0.96	0.95
Roughness length ( $z_0$ )	m	0.80	0.05	0.04	0.87	0.06
Displacement height ( $d$ )	m	1.1	0.2	0.2	12.0	0.7
Leaf area index (LAI)		4.7	0.7	2.6	6.0	5.9

Environment, <http://egis.me.go.kr/egis>) because default landuse dataset in the RAMS is out of date. The urbanized areas of Seoul and its satellite cities (number 1) are distinctive.

Tables 2 and 3 show the parameters of the LEAF and the VUCM used for the simulations, respectively. Note that the urban roughness length is assigned as the same value (0.80) in

**Table 3.** Morphological and physical parameters of the VUCM.

Parameter	Unit	Value
Roof fraction ( $f_R$ )		0.5
Canyon fraction ( $f_c$ )		0.5
Road fraction ( $f_r$ )		0.9
Vegetated area fraction ( $f_v$ )		0.1
Tree fraction ( $I_t$ )		0.7
Building height ( $h_b$ )	m	10
Tree height ( $h_t$ )	m	7.5
Canyon aspect ratio ( $h/w$ )		0.8
Roughness length for city ( $z_0$ )	m	0.8
Roof roughness length ( $z_{0R}$ )	m	0.15
Road roughness length ( $z_{0r}$ )	m	0.15
Roof albedo ( $\alpha_R$ )		0.20
Wall albedo ( $\alpha_w$ )		0.25
Road albedo ( $\alpha_r$ )		0.10
Soil albedo ( $\alpha_s$ )		soil moisture dependent
Tree albedo ( $\alpha_t$ )		0.20
Roof emissivity ( $\varepsilon_R$ )		0.94
Wall emissivity ( $\varepsilon_w$ )		0.94
Road emissivity ( $\varepsilon_r$ )		0.94
Soil emissivity ( $\varepsilon_s$ )		0.98
Tree emissivity ( $\varepsilon_t$ )		0.96
Thermal conductivity of roof ( $\kappa_R$ )	$\text{W m}^{-1} \text{K}^{-1}$	1.65
Thermal conductivity of wall ( $\kappa_w$ )	$\text{W m}^{-1} \text{K}^{-1}$	1.45
Thermal conductivity of road ( $\kappa_r$ )	$\text{W m}^{-1} \text{K}^{-1}$	1.65
Heat capacity of roof ( $C_R$ )	$\text{MJ m}^{-3} \text{K}^{-1}$	1.5
Heat capacity of wall ( $C_w$ )	$\text{MJ m}^{-3} \text{K}^{-1}$	1.5
Heat capacity of road ( $C_r$ )	$\text{MJ m}^{-3} \text{K}^{-1}$	1.9

both the simulations. The urban geometrical parameters of the VUCM such as mean building height and canyon aspect ratio are subjectively derived using the satellite imagery of the domain and their values are assigned identically to all urban patches. The building and road are assumed to be made of concrete and asphalt, respectively, whose physical properties (albedo, emissivity, conductivity, and heat capacity) are obtained from Nunez and Oke (1976) and Asaeda *et al.* (1996). Soil consists of 10 layers with a depth of 1.2 m. Soil temperatures at six vertical depths (0.05, 0.1, 0.2, 0.3, 0.5, and 1 m) measured at 20 surface meteorological stations are used for the interpolation and initialization of soil temperatures. The initial soil moisture is assumed to be 45% of saturation value of a soil type.

## 4. Results and discussion

### a. Model evaluation

There are 7 meteorological observatories (stations) and 42 automatic weather stations in the finest model domain (Fig. 5). These surface stations are a part of the operational observation network managed by the Korea Meteorological Administration (KMA). Measurement data at these 49 stations are used for model evaluation. Simulation results are compared with observed 2-m temperature and 10-m wind. Specific humidity at 3 urban stations is also compared. Comparison is made for two categories: urban and rural stations. In this study, the urban station is a station around which the urban fraction of a grid cell exceeds 80%, while the rural station is a station around which the surface is covered only with natural surfaces (non-urban landuse types). This classification yields 10 urban stations and 17 rural stations. For statistical evaluation, the mean, standard deviation, root mean square error (RMSE), and index of agreement (IOA) are calculated as follows.

$$\bar{P} = \frac{\sum_{i=1}^n P_i}{n}, \quad (5)$$

$$\sigma_p = \sqrt{\frac{\sum_{i=1}^n (P_i - \bar{P})^2}{n-1}}, \quad (6)$$

$$\text{RMSE} = \sqrt{\frac{\sum_{i=1}^n (P_i - O_i)^2}{n}}, \quad (7)$$

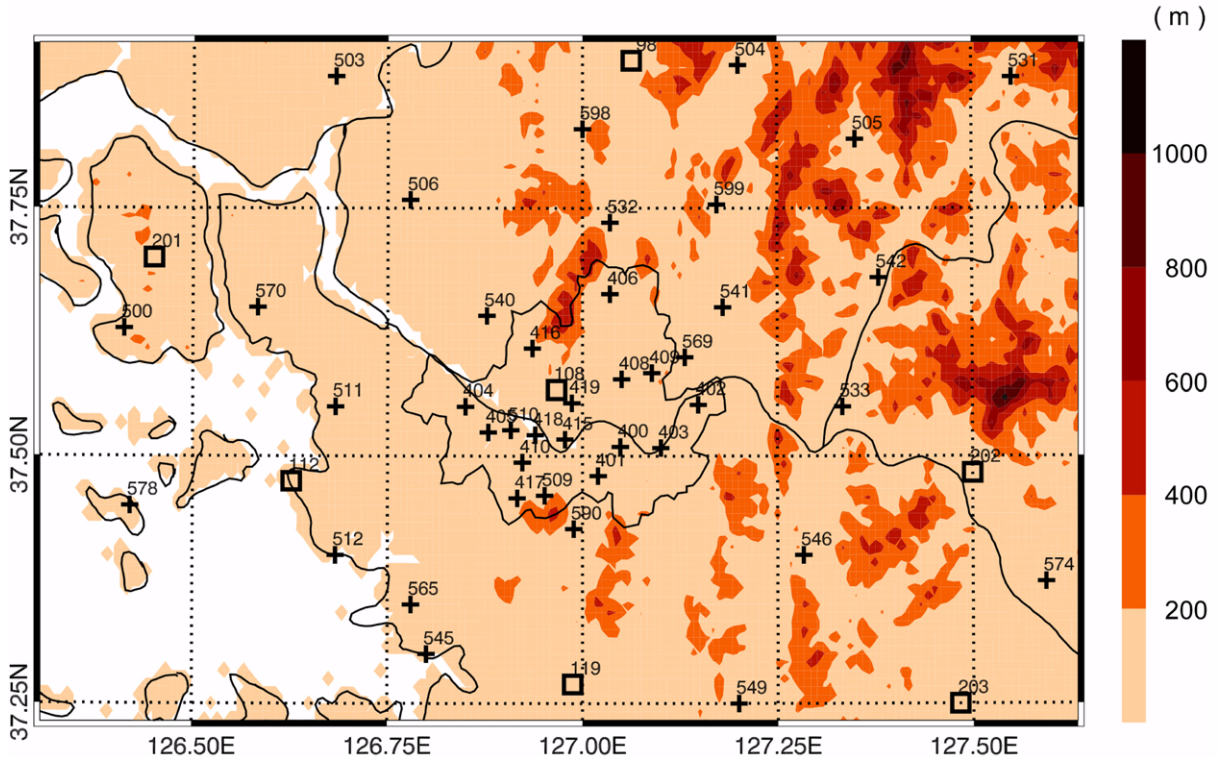


**Fig. 5.** Location of meteorological observatories (□) and automatic weather stations (+). Topography is represented by different shading tones with intervals of 200 m.

$$\text{IOA} = 1 - \frac{\sum_{i=1}^n (P_i - O_i)^2}{\sum_{i=1}^n (|P_i - \bar{O}| + |O_i - \bar{O}|)^2}, \quad (8)$$

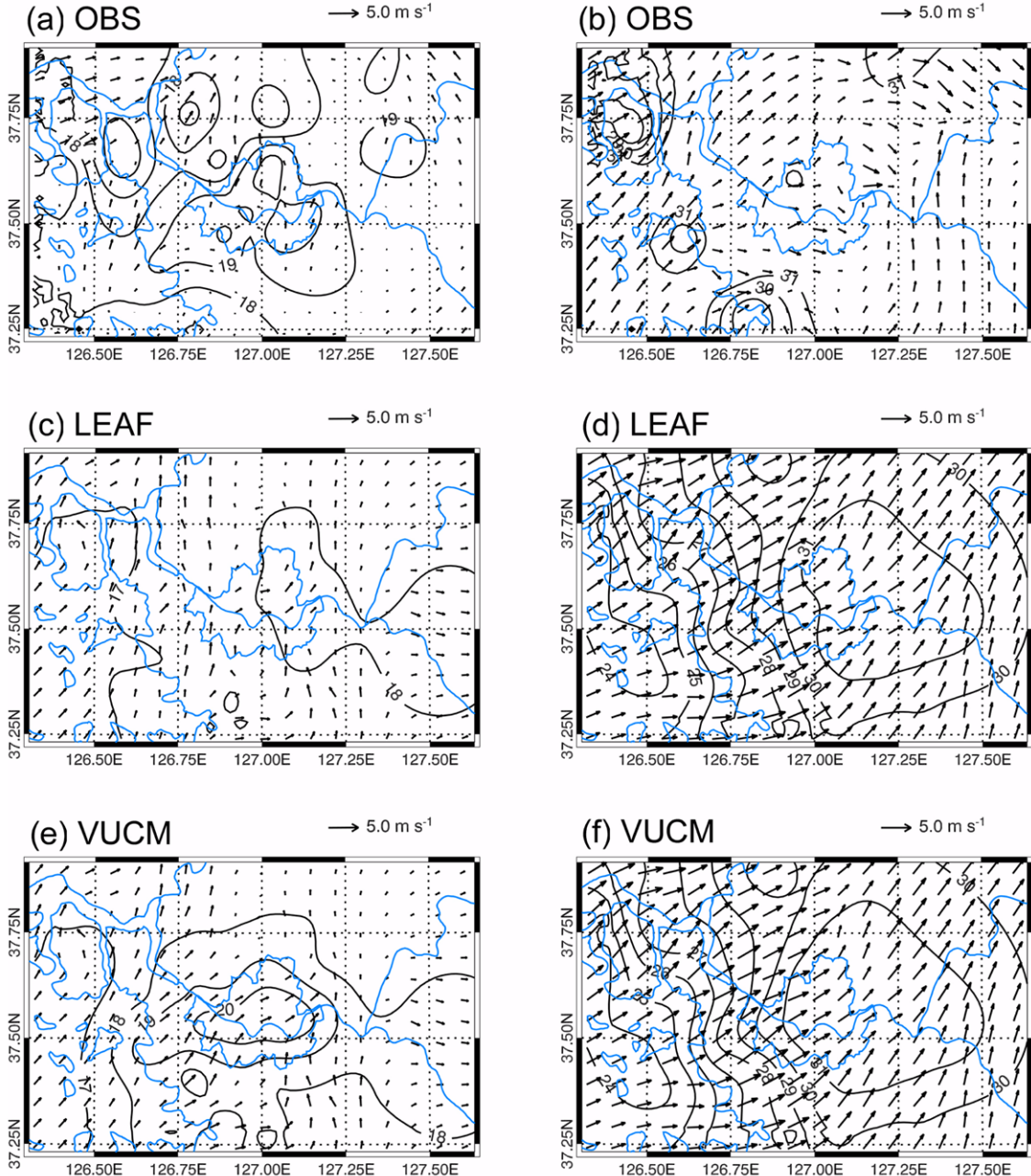
where  $n$  is the number of stations,  $P_i$  and  $O_i$  are the simulated and observed values, respectively, and the overbar indicates the mean. The IOA is a measure of relative error in a model and ranges from 0 to 1 with 0 indicating a complete disagreement and 1 indicating that the simulation is identical with the observation (Willmott, 1981).

Figure 6 shows the observed and simulated 2-m temperature and 10-m wind velocity fields at 0300 LST and 1500 LST. At 0300 LST, relatively high temperatures ranging 19–20°C are observed in Seoul, forming a UHI (Fig. 6a). Observed winds are weak, especially in Seoul. This is one of the favorable conditions for UHI formation (Kim and Baik, 2002; Lee and Baik, 2010). The UHI intensity is about 2°C. This value is smaller than the maximum UHI intensity of the day (3°C). Land breezes and confluent flows toward Seoul are not well developed in the nighttime. At 1500 LST, the temperature gradient is smeared out by well-developed sea breezes and upslope winds (Fig. 6b). Unlike in the nighttime, a warm core region in Seoul is not distinguished due to strong vertical turbulent mixing and thermal ventilation. Winds in the urban areas are relatively weak compared to those in the surrounding areas.

In the nighttime, the RAMS/VUCM is in better agreement with the observation than the RAMS/LEAF (Figs. 6c and 6e).

The RAMS/VUCM well simulates the observed UHI in Seoul. However, the RAMS/LEAF shows a spatially nearly homogeneous temperature field, thus failing to simulate the UHI in Seoul. It was analyzed in the RAMS/LEAF that the nocturnal cooling of near surface air is simulated with similar cooling rates in both the urban and rural areas. This result is inconsistent with the observed feature in Seoul (Lee and Baik, 2010). In the daytime, both the simulations show that warm air in the city is advected downstream and simultaneously relatively cold air from the sea is advected into the city by well-developed sea breezes (Figs. 6d and 6f). The temperature in Seoul is slightly higher in the RAMS/VUCM than in the RAMS/LEAF. A strong temperature gradient is formed along the coastline in both the simulations but not in the observation. This difference may be largely attributed to the fact that all surface stations are located over the land (Fig. 5). Therefore, the diurnal variation of observed near surface temperature over the sea cannot be adequately represented. Both the simulations overestimate wind speeds, especially in the urban areas. One of the causes may be relatively small roughness length for an urban patch used in the simulations. Using Geographic Information System (GIS) data, Lee *et al.* (2008) estimated a mean roughness length of 2.2 m for Seoul, which is larger than the value used for the present simulations. The sensitivities of simulated wind field to urban roughness length and other parameters deserve an investigation.

Figure 7 shows the diurnal variations of the mean, standard deviation, root mean square error, and index of agreement of 10-



**Fig. 6.** Observed and simulated 2-m temperature and 10-m wind velocity fields at 0300 LST (left panels) and 1500 LST (right panels). (a) and (b) are observations, (c) and (d) are the RAMS/LEAF simulation, and (e) and (f) are the RAMS/VUCM simulation. The contour interval in 2-m temperature fields is 1°C.

m wind averaged for 10 urban stations. The diurnal variations of wind speed and direction are well simulated in both the simulations, even though the simulations consistently overestimate wind speed by about  $0.5 \text{ m s}^{-1}$  in the afternoon (Fig. 7a). The values of standard deviation are comparable to the mean values throughout the day, implying the high spatial variations of wind speed in the urban areas (Fig. 7b). The fact that the measurement height of winds is located within the urban roughness sublayer can be responsible for the high spatial variations. However, the simulations underestimate observed spatial variations. This is

because aerodynamic parameters, especially roughness length, are applied identically to all urban patches in both the simulations. In both the simulations, the RMSE ranges from  $\sim 1 \text{ m s}^{-1}$  to  $\sim 2 \text{ m s}^{-1}$  and the IOA ranges from  $\sim 0.4$  to  $\sim 0.7$  (Figs. 7c and 7d). Even though a slight difference is found in the nighttime as a consequence of thermal forcing difference, the performance of the RAMS/LEAF and the RAMS/VUCM for winds is similar to each other. The similarity in model performance is mainly caused by the use of the same roughness length for urban patches in the two simulations.

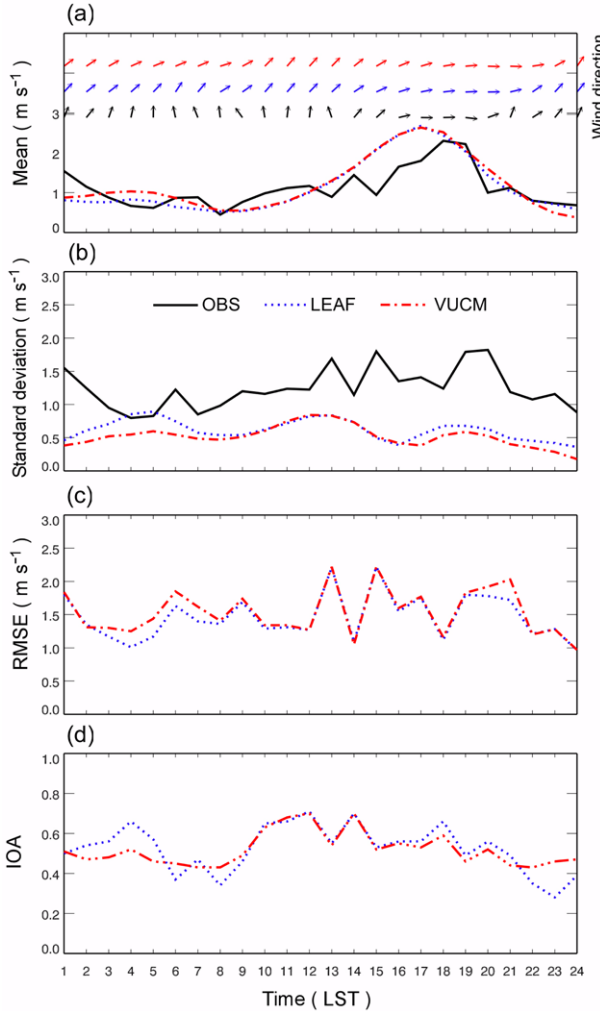


**Fig. 7.** Diurnal variations of the (a) mean, (b) standard deviation, (c) root mean square error, and (d) index of agreement of 10-m wind averaged for 10 urban stations. The arrows in (a) denote wind directions for the observation (black), the RAMS/LEAF (blue), and the RAMS/VUCM (red).

Figure 8 shows the diurnal variations of 2-m temperature statistics averaged for 10 urban stations. The RAMS/VUCM well simulates the observed diurnal variation of 2-m temperature, while the RAMS/LEAF greatly underestimates the temperature throughout the day (Fig. 8a). There is about one hour time lag in peak temperature between the simulations. This can be explained through surface energy balance analysis given in the following subsection. In both the simulations, spatial variations are reasonably compared to the observed (Fig. 8b). The model performance for near surface temperature is significantly improved by the implementation of the VUCM, especially in the nighttime (Figs. 8c and 8d).

Figure 9 shows the scatter plots of the observed versus simulated 2-m temperatures averaged for 10 urban, 17 rural, and all 49 stations. In each panel, a linear regression equation and  $f$  value are given. Here,  $f$  value indicates the percentage of simulated temperatures within  $\pm 2^\circ\text{C}$  of observed ones. For the

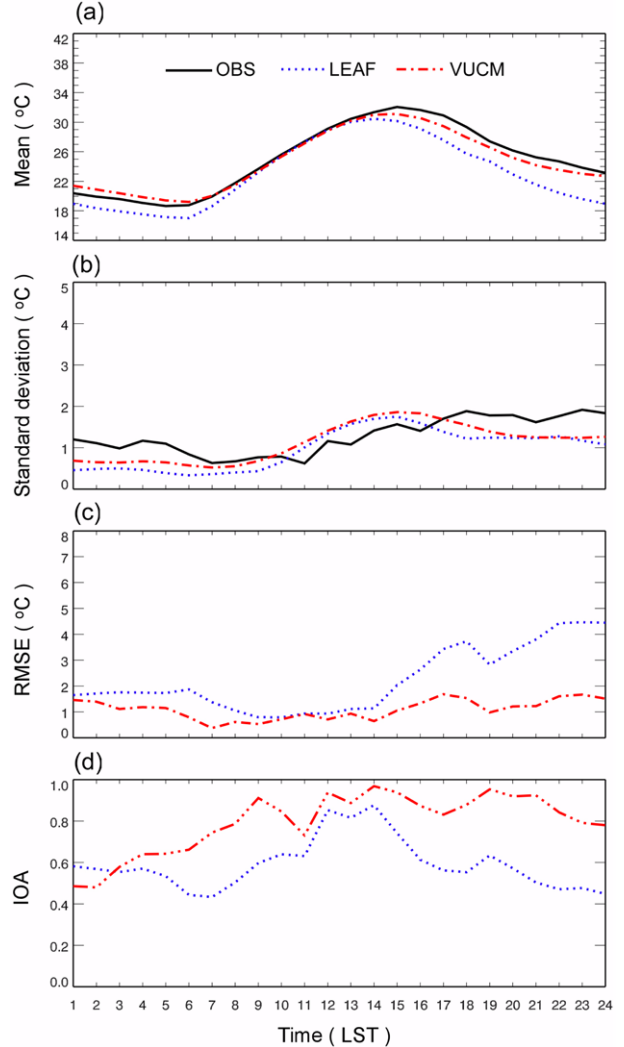


**Fig. 8.** Diurnal variations of the (a) mean, (b) standard deviation, (c) root mean square error, and (d) index of agreement of 2-m temperature averaged for 10 urban stations.

urban stations,  $f$  value is 58.3% in the RAMS/LEAF, while it is as large as 91.7% in the RAMS/VUCM (Figs. 9a and 9b). For the rural stations, there is a slight improvement in the RAMS/VUCM (Figs. 9c and 9d). The significant improvement for the urban stations mainly contributes to the improvement shown in comparison for all the stations (Figs. 9e and 9f). These results indicate that appropriate parameterizations of urban physical processes are required for better simulations of the urban atmosphere.

Figure 10 shows the diurnal variations of the observed and simulated specific humidities at three urban stations (Seoul, Incheon, and Suwon). The observed specific humidity is calculated using observed relative humidity, temperature, and pressure. At two inland stations (Seoul and Suwon), a similar diurnal variation pattern is found (Figs. 10a and 10c). The specific humidity decreases in the morning as the UBL deepens. The specific humidity rapidly increases after around 1500–1600 LST when sea breezes influence the regions. The specific

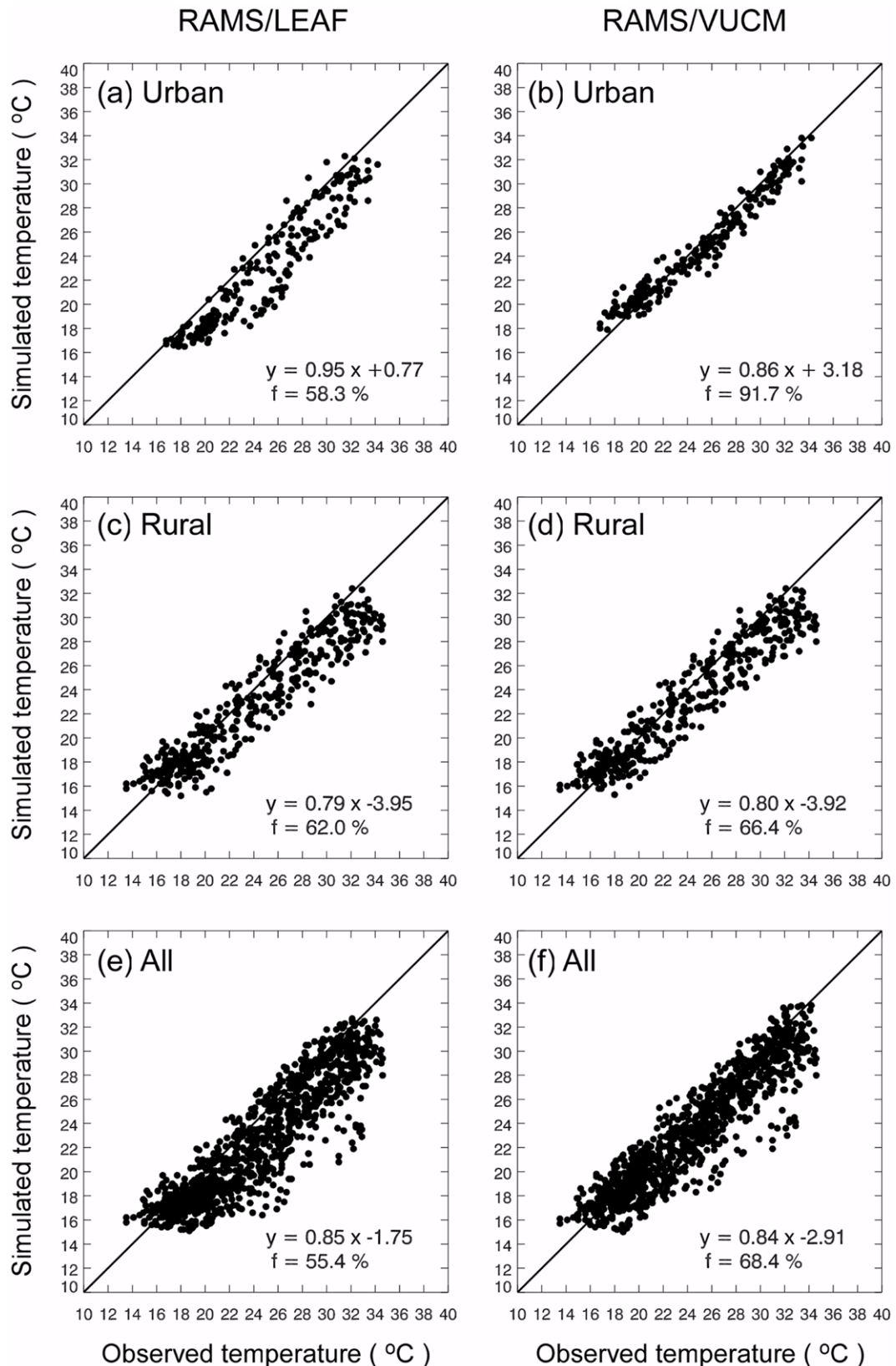


**Fig. 9.** Scatter plots of the observed versus simulated 2-m temperatures for 10 urban stations [(a) and (b)], 17 rural stations [(c) and (d)], and all 49 stations [(e) and (f)]. Left panels are for the RAMS/LEAF, and right panels are for the RAMS/VUCM. In each panel, a linear regression equation and *f* value are given.

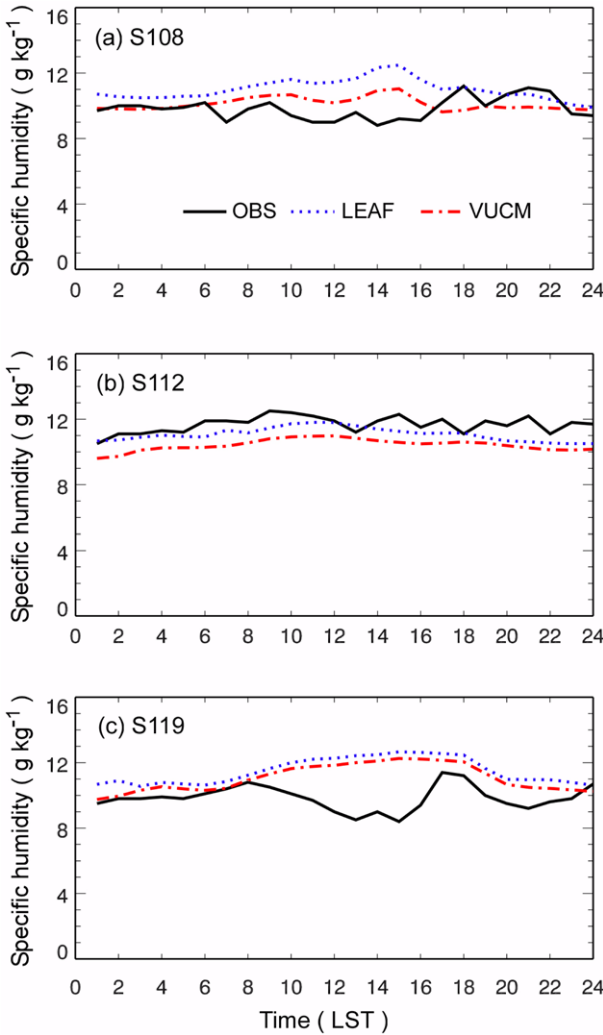


**Fig. 10.** Diurnal variations of the observed and simulated specific humidities at (a) Seoul, (b) Incheon, and (c) Suwon meteorological stations. Station locations are indicated by □ with station numbers 108, 112, and 119 in Fig. 5, respectively.

humidity at a coastal station (Incheon) shows a small diurnal variation, keeping relatively high specific humidity compared to the inland stations (Fig. 10b). The simulations overestimate the observation at the two inland stations, while the simulated specific humidity at the coastal station is underestimated. At the three stations, the simulated specific humidity by the RAMS/VUCM is smaller by about 1–2 g kg<sup>−1</sup> than that by the RAMS/LEAF throughout the day. This difference is associated with larger Bowen ratios in the RAMS/VUCM than in the RAMS/LEAF in the urban areas, as will be shown in the next subsection.

### b. Urban surface energy balance

A surface energy balance equation can be given by

$$Q^* + Q_F = Q_H + Q_E + \Delta Q_s \quad (9)$$

where  $Q^*$  is the net radiative flux,  $Q_F$  is the anthropogenic heat

flux,  $Q_H$  is the sensible heat flux,  $Q_E$  is the latent heat flux, and  $\Delta Q_s$  is the storage heat flux. The analysis is focused on differences in surface energy balance between the RAMS/VUCM and the RAMS/LEAF. Figure 11 shows simulated surface energy balance fluxes averaged for the urban stations, together with corresponding fluxes averaged for the rural stations. In general, the energy partitioning at an urban surface is significantly different from that at a natural surface mainly due to differences in thermal inertia and moisture availability. The simulation results show that the sensible heat flux (latent heat flux) in the urban areas is larger (smaller) than that in the rural areas (Figs. 11b and 11c) and that the storage heat flux in the urban areas is larger than that in the rural areas (Fig. 11d). These results are qualitatively consistent with those of previous studies (Grimmond, 2007; Holt and Pullen, 2007).

In addition to the differences between the urban and rural areas, differences in surface energy balance between the RAMS/VUCM and the RAMS/LEAF are also distinctive. Note that the chosen urban stations contain natural surfaces with their fractions less than 20%. Therefore, the differences are mainly caused by the different urban parameterizations. The daytime net radiative flux in the RAMS/VUCM is smaller up to about 50 W m<sup>−2</sup> around noon than that in the RAMS/LEAF (Fig. 11a). This is attributed to relatively high urban albedo and large upward longwave radiation in the RAMS/VUCM. In addition, enhanced upward longwave radiation by high surface temperature results in strong nocturnal radiative cooling in the RAMS/VUCM. The daytime sensible heat flux in the RAMS/VUCM is larger than that in the RAMS/LEAF, and its peak value is delayed by about two hours (Fig. 11b). The time lag is consistent with the 2-m temperature variation in Fig. 8. The daytime latent heat flux in the RAMS/VUCM is much lower by about 200 W m<sup>−2</sup> around noon than that in the RAMS/LEAF (Fig. 11c). Relatively small latent heat flux in the RAMS/VUCM is mainly due to reduced moisture availability in urban surfaces, by which the reduction in near surface specific humidity (Fig. 10) can be explained. The daytime storage heat flux in the RAMS/VUCM is also larger than that in the RAMS/LEAF, and its sign change in the late afternoon appears about one hour later than that in the RAMS/LEAF (Fig. 11d).

In the RAMS/VUCM, as a consequence of small  $Q_E/Q^*$ , the daytime  $Q_H/Q^*$  is 0.49,  $\Delta Q_s/Q^*$  is 0.42, and the Bowen ratio ( $= Q_H/Q_E$ ) is 5.4. These values are comparable to the observation in a light industrial area in Vancouver, Canada (Oke *et al.*, 1999). The nocturnal energy balance shows that  $Q_H/Q^*$  is −0.28 and  $\Delta Q_s/Q^*$  is 1.28 in the RAMS/VUCM. The large  $\Delta Q_s/Q^*$  results from the large daytime  $\Delta Q_s$  at the urban surfaces. This characteristic nocturnal energy balance retards near surface temperature decrease, consequently helping to form a nocturnal UHI. However, the nocturnal radiative cooling is almost exactly balanced with  $\Delta Q_s$  ( $\Delta Q_s/Q^* = 1.01$ ) in the RAMS/LEAF as is in natural surfaces.

The magnitude of the nighttime anthropogenic heat flux is comparable to that of the sensible heat flux (Fig. 11b). Therefore, the inclusion of anthropogenic heat flux may contribute to the

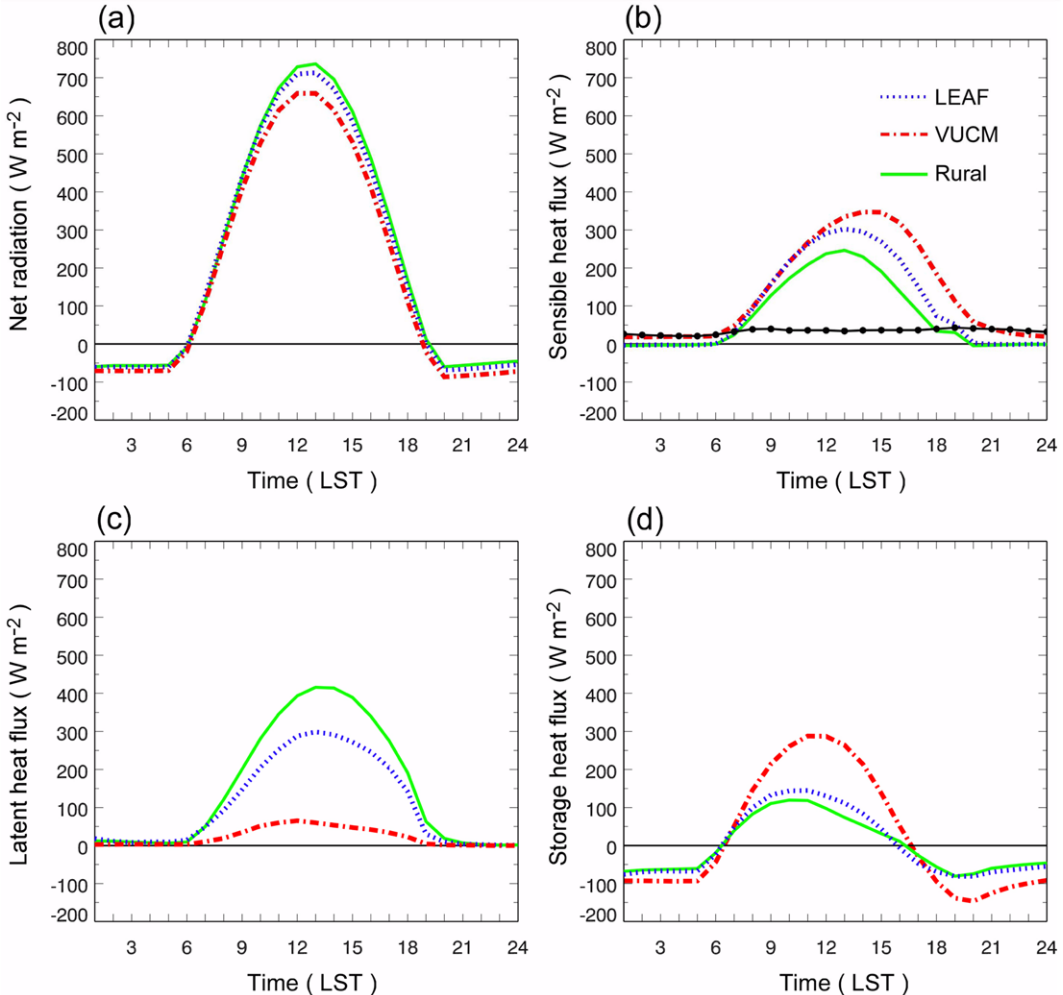


**Fig. 11.** Diurnal variations of the simulated surface energy balance fluxes averaged for the urban stations and the rural stations. The dotted and dashed-dotted lines indicate urban surface energy balance fluxes simulated by the RAMS/LEAF and the RAMS/VUCM, respectively. The storage heat flux is calculated as a residual. The solid line with dots in (b) represents the anthropogenic heat flux (from Lee *et al.*, 2009) averaged for the urban stations.

surface energy balance in the urban areas by modulating atmospheric stability and turbulence intensity. The surface energy balance cycle in the RAMS/VUCM is similar to the observation in highly urbanized areas (Oke *et al.*, 1999; Lemonus *et al.*, 2004).

#### c. Urban boundary layer

The UBL can be significantly influenced by surface turbulent heat fluxes. Given horizontally homogeneous conditions, the UBL depth is proportional to the time-integrated surface sensible heat flux and inversely proportional to atmospheric stability. The breakdown process of a nocturnal inversion layer is also highly associated with surface heat fluxes along with mechanical turbulence effects such as entrainment (Garratt, 1992). Therefore, the UBL is one of the resultant structures formed as a response to surface energy exchange processes.

Figure 12 shows the longitude-height cross-sections at 37.5°N

of potential temperature and wind velocity at 1400 LST and 2400 LST simulated by the RAMS/VUCM and their differences between the RAMS/VUCM and the RAMS/LEAF. At 1400 LST, sea breezes develop well and advance over the city. Moreover, two thermal internal boundary layer structures are found in the transition areas. One is at 126.4°E where changes from the sea to the island surfaces occur, and the other is at 126.6°E where changes from the inland natural surfaces to the urban areas occur (Fig. 12a). The penetration of sea breeze front is retarded by about 10 km due to its interaction with the urban surfaces. The implementation of the VUCM increases potential temperature in the UBL up to 0.7°C. Consequently, weak urban-induced winds appear as a response to the thermal forcing (Fig. 12b). At 2400 LST, the simulated atmosphere is weakly unstable in the RAMS/VUCM with UBL heights of about 100–200 m (Fig. 12c). The potential temperature in the RAMS/VUCM is warmer by 1–2°C than that in the RAMS/LEAF in the urban areas (Fig. 12d). Urban-induced winds associated with

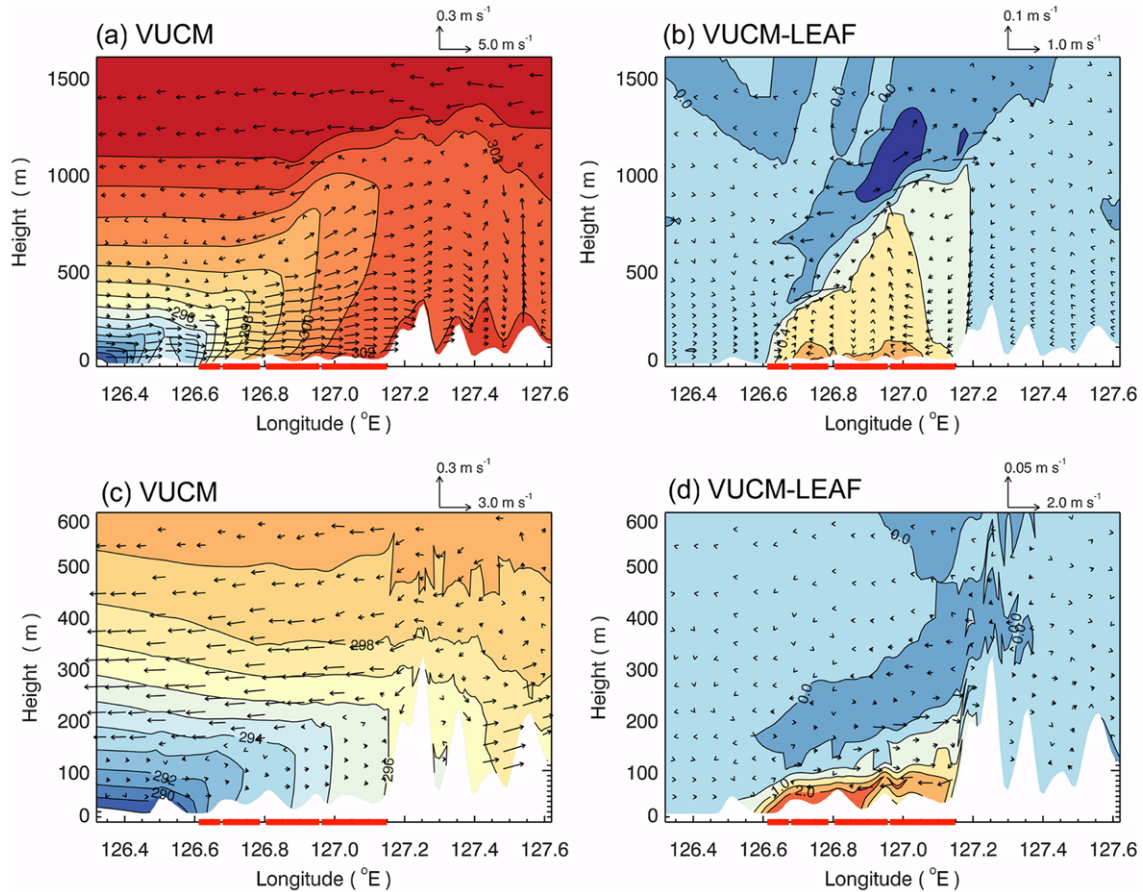


**Fig. 12.** Longitude-height cross-sections at 37.5°N of the simulated potential temperature and wind velocity at (a) 1400 LST and (c) 2400 LST in the RAMS/VUCM. Right panels represent differences between the RAMS/VUCM and RAMS/LEAF simulations at (b) 1400 LST and (d) 2400 LST. Urban areas are represented by thick lines on the longitude axis. The contour interval is 1°C in (a) and (c), 0.2°C in (b), and 0.5°C in (d).

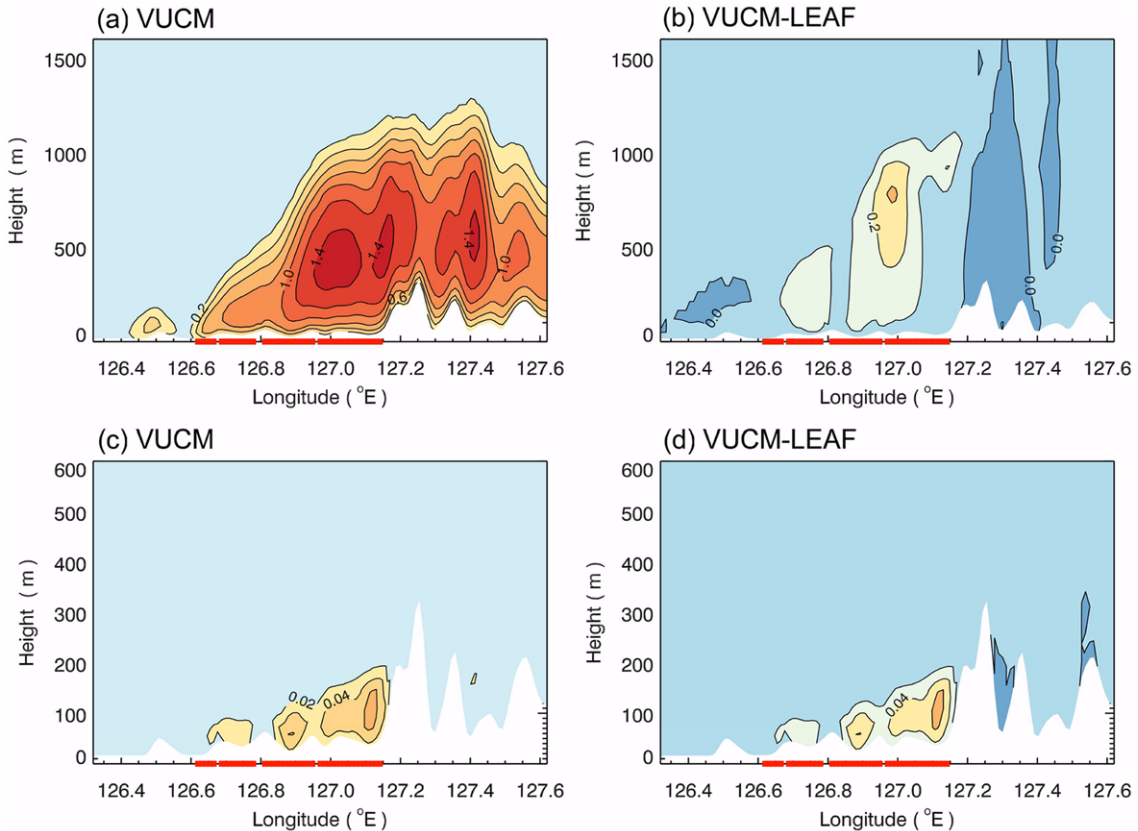
the thermal forcing are relatively stronger in the nighttime than in the daytime. The impacts of the VUCM in the nighttime are restricted to a shallow layer of about 100 m in the simulation.

Figure 13 shows the longitude-height cross-sections at 37.5°N of TKE at 1400 LST and 2400 LST simulated by the RAMS/VUCM and TKE differences between the RAMS/VUCM and the RAMS/LEAF. At 1400 LST, strong turbulence activity appears in the urban areas and inland mountain areas in the RAMS/VUCM, exhibiting typical convective boundary layer structures. The influence of sea breezes, characterized by colder and more stable air, is clear in the urban areas with a relatively lower UBL height (Fig. 13a). The turbulence intensity in the urban areas is slightly enhanced by the implementation of the VUCM, but its impact is relatively small (Fig. 13b). At 2400 LST, weak turbulence exists with a maximum TKE of 0.06 m<sup>2</sup> s<sup>-2</sup> in the urban areas (Fig. 13c). The nocturnal UBL in the RAMS/VUCM is slightly unstable, leading to a UBL depth of about 100–200 m by positive sensible heat flux. These characteristic features of the UBL in the RAMS/VUCM are comparable to the observed UBL in highly urbanized cities (Dupont *et al.*, 1999; Mestayer *et al.*, 2005). However, the nocturnal UBL in the RAMS/LEAF is found to be very stable, even in the

urban areas, and thus the TKE is strongly suppressed, resulting in a poor performance in the UHI simulation. The impacts of the VUCM are positive in the surface energy balance and the UBL formation, and its impacts are more distinctive in the nighttime when a shallow UBL forms.

## 5. Summary and conclusions

The vegetated urban canopy model (VUCM), which includes various important urban physical processes, was implemented in the mesoscale meteorological model RAMS. The coupled model RAMS/VUCM was evaluated and then used to examine its impacts on the urban boundary layer (UBL) in the Seoul metropolitan area. The comparison with observations shows that the RAMS/VUCM well simulates the spatial pattern of the nocturnal urban heat island (UHI) in Seoul. However, the RAMS/LEAF fails to simulate the UHI formation by exhibiting strong cold biases in the nighttime. A statistical evaluation of 2-m temperature shows that the model performance is significantly improved by the VUCM, especially in the nighttime. About 92% of simulated temperatures in the RAMS/VUCM are within ± 2°C of observed ones in the urban areas, while only about 58% exist



**Fig. 13.** Longitude-height cross-sections at 37.5°N of the simulated turbulent kinetic energy (TKE) at (a) 1400 LST and (c) 2400 LST in the RAMS/VUCM. Right panels represent differences between the RAMS/VUCM and RAMS/LEAF simulations at (b) 1400 LST and (d) 2400 LST. The contour interval is 0.2 m<sup>2</sup> s<sup>-2</sup> in (a), 0.1 m<sup>2</sup> s<sup>-2</sup> in (b), and 0.02 m<sup>2</sup> s<sup>-2</sup> in (c) and (d).

within the range in the RAMS/LEAF. However, an improvement in wind field is not achieved in the simulation. The specific humidity in the RAMS/VUCM is lower by about 1-2 g kg<sup>-1</sup> than that in the RAMS/LEAF in the urban areas due to less moisture availability. The RAMS/VUCM shows characteristic features in urban surface energy balance such as large Bowen ratio, nocturnal upward sensible heat flux, and large storage heat flux. A weakly unstable nocturnal UBL with heights of about 100-200 m forms in the RAMS/VUCM. These results are well compared with many field measurements in highly urbanized areas. Furthermore, a better performance in 2-m temperature is associated with the realistic simulation of surface energy partitioning. However, the diurnal variations of urban surface energy balance fluxes in the RAMS/LEAF are similar to those in the natural surfaces, thus failing to simulate the UHI formation.

In this study, the input parameters of the VUCM are assigned as representative values identically for all urban patches. This may be partly responsible for the small spatial variations of near surface winds in the simulation compared to the observation. For more realistic simulation, a representation of heterogeneity in urban morphology using high resolution urban morphological database will be necessary. In addition to the input parameters of the VUCM, the anthropogenic heat flux with temporal and spatial variations, which is available for the Seoul metropolitan

area by Lee *et al.* (2009), needs to be considered.

**Acknowledgements.** The authors are very grateful to two anonymous reviewers for providing valuable comments on this work. This work was funded by the Korea Meteorological Administration Research and Development Program under Grant RACS 2010-4005 and the Brain Korea 21 Project.

## REFERENCES

- Allwine, K. J., J. H. Shinn, G. E. Streit, K. L. Clawson, and M. Brown, 2002: Overview of URBAN 2000: A multiscale field study of dispersion through an urban environment. *Bull. Amer. Meteor. Soc.*, **83**, 521-536.
- Asaeda, T., V. T. Ca, and A. Wake, 1996: Heat storage of pavement and its effect on the lower atmosphere. *Atmos. Environ.*, **30**, 413-427.
- Avissar, R., and R. A. Pielke, 1989: A parameterization of heterogeneous land surfaces for atmospheric numerical models and its impact on regional meteorology. *Mon. Wea. Rev.*, **117**, 2113-2136.
- Best, M. J., C. S. B. Grimmond, and M. G. Villani, 2006: Evaluation of the urban tile in MOSES using surface energy balance observations. *Bound.-Layer Meteor.*, **118**, 503-525.
- Chen, C., and W. R. Cotton, 1983: A one-dimensional simulation of the stratocumulus-capped mixed layer. *Bound.-Layer Meteor.*, **25**, 289-321.
- Davies, H. C., 1976: A lateral boundary formulation for multi-level prediction models. *Quart. J. Roy. Meteor. Soc.*, **102**, 405-418.
- Deardorff, J. W., 1978: Efficient prediction of ground surface temperature

- and moisture, with inclusion of a layer of vegetation. *J. Geophys. Res.*, **83(C4)**, 1889-1903.
- Dickinson, R. E., M. Shaikh, R. Bryant, and L. Graumlich, 1998: Interactive canopies for a climate model. *J. Climate*, **11**, 2823-2836.
- Dupont, E., L. Menut, B. Carissimo, J. Pelon, and P. Flamant, 1999: Comparison between the atmospheric boundary layer in Paris and its rural suburbs during the ECLAP experiment. *Atmos. Environ.*, **33**, 979-994.
- Feigenwinter, C., R. Vogt, and E. Parlow, 1999: Vertical structure of selected turbulence characteristics above an urban canopy. *Theor. Appl. Climatol.*, **62**, 51-63.
- Garratt, J. R., 1992: *The atmospheric boundary layer*. Cambridge University Press, 316 pp.
- Grimmond, C. S. B., 2007: Urbanization and global environmental change: Local effects of urban warming. *Geogr. J.*, **173**, 83-88.
- \_\_\_\_\_, and T. R. Oke, 2002: Turbulent heat fluxes in urban areas: Observations and a local-scale urban meteorological parameterization scheme (LUMPS). *J. Appl. Meteor.*, **41**, 792-810.
- Helfand, H. M., and J. C. Labraga, 1988: Design of a nonsingular level 2.5 second-order closure model for the prediction of atmospheric turbulence. *J. Atmos. Sci.*, **45**, 113-132.
- Holt, T., and J. Pullen, 2007: Urban canopy modeling of the New York city metropolitan area: A comparison and validation of single- and multilayer parameterization. *Mon. Wea. Rev.*, **135**, 1906-1930.
- Jiang, H., and W. R. Cotton, 2000: Large eddy simulation of shallow cumulus convection during BOMEX: Sensitivity to microphysics and radiation. *J. Atmos. Sci.*, **57**, 582-594.
- Kastner-Klein, P., E. Fedorovich, and M. W. Rotach, 2001: A wind tunnel study of organised and turbulent air motions in urban street canyons. *J. Wind Eng. Ind. Aerodyn.*, **89**, 849-861.
- Kim, Y.-H., and J.-J. Baik, 2002: Maximum urban heat island intensity in Seoul. *J. Appl. Meteor.*, **41**, 651-659.
- Kusaka, H., H. Kondo, Y. Kikegawa, and F. Kimura, 2001: A simple single-layer urban canopy model for atmospheric models: Comparison with multi-layer and slab models. *Bound.-Layer Meteor.*, **101**, 329-358.
- Lee, H. W., H.-J. Choi, S.-H. Lee, Y.-K. Kim, and W.-S. Jung, 2008: The impact of topography and urban building parameterization on the photochemical ozone concentration of Seoul, Korea. *Atmos. Environ.*, **42**, 4232-4246.
- Lee, S.-H., and S.-U. Park, 2008: A vegetated urban canopy model for meteorological and environmental modelling. *Bound.-Layer Meteor.*, **126**, 73-102.
- \_\_\_\_\_, and J.-J. Baik, 2010: Statistical and dynamical characteristics of the urban heat island intensity in Seoul. *Theor. Appl. Climatol.*, **100**, 227-237.
- \_\_\_\_\_, C.-K. Song, J.-J. Baik, and S.-U. Park, 2009: Estimation of anthropogenic heat emission in the Gyeong-In region of Korea. *Theor. Appl. Climatol.*, **96**, 291-303.
- Lee, T. J., and R. A. Pielke, 1992: Estimating the soil surface specific humidity. *J. Appl. Meteor.*, **31**, 480-484.
- Lemonsu, A., C. S. B. Grimmond, and V. Masson, 2004: Modeling the surface energy balance of the core of an old Mediterranean city: Marseille. *J. Appl. Meteor.*, **43**, 312-327.
- Lyons, W. A., R. A. Pielke, C. J. Tremback, R. L. Walko, D. A. Moon, and C. S. Keen, 1995: Modeling impacts of mesoscale vertical motions upon coastal zone air pollution dispersion. *Atmos. Environ.*, **29**, 283-301.
- Martilli, A., A. Clappier, and M. W. Rotach, 2002: An urban surface exchange parameterisation for mesoscale models. *Bound.-Layer Meteor.*, **104**, 261-304.
- Masson, V., 2000: A physically-based scheme for the urban energy budget in atmospheric models. *Bound.-Layer Meteor.*, **94**, 357-397.
- McQueen, J. T., R. A. Valigura, and B. J. B. Stunder, 1997: Evaluation of the RAMS model for estimating turbulent fluxes over the Chesapeake Bay. *Atmos. Environ.*, **31**, 3803-3819.
- Mestayer, P. G., and Coauthors, 2005: The urban boundary-layer field campaign in Marseille (UBL/CLU-ESCOMPTE): Set-up and first results. *Bound.-Layer Meteor.*, **114**, 315-365.
- Nunez, M., and T. R. Oke, 1976: Long-wave radiative flux divergence and nocturnal cooling of the urban atmosphere. *Bound.-Layer Meteor.*, **10**, 121-135.
- Oke, T. R., R. A. Spronken-Smith, E. Jauregui, and C. S. B. Grimmond, 1999: The energy balance of central Mexico City during the dry season. *Atmos. Environ.*, **33**, 3919-3933.
- Oleson, K. W., G. B. Bonan, J. Feddema, M. Vertenstein, and C. S. B. Grimmond, 2008: An urban parameterization for a global climate model. Part I: Formulation and evaluation for two cities. *J. Appl. Meteor. Climatol.*, **47**, 1038-1060.
- Pielke, R. A., and Coauthors, 1992: A comprehensive meteorological modeling system-RAMS. *Meteor. Atmos. Phys.*, **49**, 69-91.
- Sellers, P. J., D. A. Randall, G. J. Collatz, J. A. Berry, C. B. Field, D. A. Dazlich, C. Zhang, G. D. Collelo, and L. Bounoua, 1996: A revised land surface parameterization (SiB2) for atmospheric GCMs. Part I: Model formulation. *J. Climate*, **9**, 676-705.
- Tremback, C. J., 1990: Numerical simulation of a mesoscale convective complex: Model development and numerical results. Ph.D. dissertation, Colorado State University, 247 pp.
- United Nations, 2004: World urbanization prospects: The 2003 revision. United Nations Department of Economic and Social Affairs, 34 pp. [Available online at [http://www.un.org/esa/population/publications/wup\\_2003/2003Highlights.pdf](http://www.un.org/esa/population/publications/wup_2003/2003Highlights.pdf).]
- Walko, R. L., and Coauthors, 2000: Coupled atmosphere-biophysics-hydrology models for environmental modeling. *J. Appl. Meteor.*, **39**, 931-944.
- Willmott, C. J., 1981: On the validation of models. *Phys. Geogr.*, **2**, 184-194.
- Zhong, S., and J. Fast, 2003: An evaluation of the MM5, RAMS and Meso-Eta models at subkilometer resolution using VTMX field campaign data in the Salt Lake valley. *Mon. Wea. Rev.*, **131**, 1301-1322.